



## Regular paper

## A wideband reconfigurable folded planar dipole using MEMS and hybrid polymeric substrates

Herwansyah Lago<sup>a,b,\*</sup>, Zahriladha Zakaria<sup>b</sup>, Mohd Faizal Jamlos<sup>c</sup>, Ping Jack Soh<sup>d</sup><sup>a</sup> Faculty of Engineering, Universiti Malaysia Sabah, 88400 Kota Kinabalu, Sabah, Malaysia<sup>b</sup> Centre of Telecommunication Research and Innovation (CeTRI), Faculty of Electronic and Computer Engineering, Universiti Teknikal Malaysia Melaka (UTeM), Malaysia<sup>c</sup> Faculty of Mechanical Engineering, Universiti Malaysia Pahang, 26600 Pekan, Malaysia<sup>d</sup> Advanced Communication Engineering Centre (ACE) CoE, School of Computer & Communication Engineering, Universiti Malaysia Perlis, Malaysia

## ARTICLE INFO

## Article history:

Received 23 July 2018

Accepted 15 December 2018

## Keywords:

Wideband  
Hybrid polymeric  
Reconfigurable  
RF MEMS

## ABSTRACT

A wideband reconfigurable folded planar dipole using hybrid polymeric substrates is proposed. Artificial Magnetic Conductor (AMC) is a periodic structure composed of rectangular patches integrated with Jerusalem Cross (JSC) slots and being located in between two substrates. The Perfect Magnetic Conductor (PMC)-like behaviour of the AMC structure enabled the printed folded dipole to be placed near to the proposed structure, resulting in a low-profile antenna with 5.11 dB gain operating at 9.41 GHz. The combined use of the polymeric substrate and the proposed AMC resulted in a 1 GHz of bandwidth. The proposed antenna is capable in beam steering on the  $xz$ -plane via the integration of radio frequency (RF) MEMS switches placed on the antenna feeding transmission line. Simulations and measurements show a satisfactory agreement, with a beam steering capability at least  $30^\circ$ , bandwidth of 1 GHz and maximum gain of 5.11 dB.

© 2018 Elsevier GmbH. All rights reserved.

## 1. Introduction

In recent years, the developments towards reconfigurable antenna have received significant attention among researchers owing to its aptitude in fulfilling the demands of smart communication systems. Generally, a reconfigurable antenna is tuneable in terms of operating frequency, polarization or radiation pattern. Moreover, any undesired signal source can be avoided by radiation pattern manipulation [1].

Designing an effective beam-reconfigurable antenna is challenging due to components' losses, especially from RF switches. Several proposed methods by recent researchers to realize reconfigurability feature are such as by altering the antenna's physical structure [2]. Another method to integrate beam-reconfigurable capability is by modifying the material properties [3], for instance, a voltage-controlled substrate can be used to realize pattern reconfigurability via biasing [3]. The next method for the same purpose is by controlling the feed and surface current on the radiating elements. This can be effectively done by integrating radio frequency (RF) switches with antennas [4–12]. Among the popular RF switch are PIN diodes, FETs and RF MEMS.

Recently, PIN diodes were used to achieve beam pattern reconfigurability on printed quasi-yagi antenna [13] and to enable parasitic tuning in [14]. However, the presence of the PIN diodes caused efficiency degradation [15]. Moreover, PIN diodes are restricted in term of power handling capability, insertion loss, isolation, high operating frequency and high gain [16]. An effective alternative proposed in [7,9–10,17–20] is the micro-electro-mechanical system (MEMS). This is mainly due to its better insertion losses, isolation, and power handling capability at high frequency [19]. Moreover, the matching issue faced by other solutions such as PIN diodes is non-existent for MEMS due to the existing 50 Ohm transmission line behaviour during its active state [17].

Besides beam-reconfigurability, another desirable antenna feature is a high front-to-back ratio (FBR). Metamaterials, also known as metasurfaces in two-dimensional form, have been identified as the most effective method for FBR enhancement. Metamaterials can be classified into several types: high impedance surface (HIS) [21,22], electromagnetic band-gap (EBG) ground plane [23,24], reactive impedance substrate (RIS) [25], and artificial magnetic conductor (AMC) [19,26–28]. The AMC surface proposed in [27] improved the antenna bandwidth, besides enabling it to be placed near to the main radiator element and act as an additional reflector. This is due to the AMC's current behaviour, which exhibit the characteristics of an in-phase image [27]. However, AMC structure is typically bandwidth-limited, defined by its  $\pm 45^\circ$  phase response.

\* Corresponding author.

E-mail addresses: [herwansyah@ums.edu.my](mailto:herwansyah@ums.edu.my) (H. Lago), [zahriladha@utem.edu.my](mailto:zahriladha@utem.edu.my) (Z. Zakaria), [mohdfaizaljamlos@gmail.com](mailto:mohdfaizaljamlos@gmail.com) (M.F. Jamlos), [pjsoh@unimap.edu.my](mailto:pjsoh@unimap.edu.my) (P.J. Soh).

This limits its application in covering the whole radio navigation and location-tracking channel in X-band. An interesting and effective option is by employing polymeric substrates to improve antenna's bandwidth [29]. Furthermore, polymeric substrates are advantageous due to its simple fabrication process and the availability of this process in-house. Its physical and material properties can also be easily adjusted to suit the requirements in terms of thickness, width and length. Besides that, the material properties of the polymeric substrate can also be altered by mixing with others composites as presented in [30].

From the initial work reported in [31], this investigation has been expanded to include practical integration and experimental results of the three components: an AMC layer, a Polydimethylsiloxane (PDMS) polymeric substrate and the RF MEMS switching mechanism. All three components are optimized to result in significant improvements of the overall antenna, especially in terms of operating bandwidth, gain and tilting angle. A bandwidth of up to 1 GHz (10.6%) is achieved, in addition to its capability of beam-steering of at least  $30^\circ$  on the  $xz$ -plane with a maximum gain of 5.11 dB. Most importantly, the integration of the polymeric substrate also enabled its compact physical structure of  $1.59\lambda \times 0.86\lambda \times 0.12\lambda$ . To our best knowledge, this is the first prototyped and measured reconfigurable MEMS antenna combined with the use of polymeric substrate to result in consistent switched beams and gains, besides a broad bandwidth.

This paper is organized as follows. The structure and performance of several types of the AMC planes will be first presented and evaluated. Next, the integration of the AMC plane on the presented antenna structure will then be studied in Section 2. This is then followed by the analysis of the level of bandwidth improvement via the use of the PDMS substrate with the antenna in the Sections 3 and 4. Finally, the conclusions from this work are drawn in the Section 5.

## 2. AMC design and evaluation

The AMC design starts by defining and analysing the phase and magnitude response of the AMC unit cell. The AMC is ideally lossless at the desired frequency, while the phase of a reflected wave is  $0^\circ$ . The AMC bandwidth is determined within  $\pm 45^\circ$  of this phase [22]. Fig. 1(a) depicts the proposed structure of the AMC unit cell. The AMC unit cell consists of four layers: two layers of substrates, a layer of AMC and ground respectively. A full ground plane is located at the bottom-most layer of the antenna, followed by the

PDMS and Taconic substrate. The AMC unit cell is placed between the Taconic substrate and the PDMS polymeric substrate, while the radiator is placed on the top-most layer. Both the AMC and ground plane are formed using copper with a thickness of 0.035 mm. The Taconic TLY-5 substrate used is 1.5748 mm in thickness, with a dielectric constant ( $\epsilon_{r1}$ ) of 2.2 and loss tangent ( $\tan\delta$ ) of 0.006. Meanwhile, a 2 mm-thick PDMS is used, and its dielectric constant ( $\epsilon_{r2}$ ) and loss tangent is 2.7 and 0.009, respectively.

Three popular AMC unit cells operating at 9.41 GHz are evaluated in this work, a rectangular, a cross-shaped and a Jerusalem Cross (JSC)-shaped unit cell, see Fig. 1(b). In contrast to previous literature, the layer structure in this work is combined with the proposed polymeric (PDMS) substrate as depicted in Fig. 1(a). Each unit cell is sized at  $8.85 \times 8.85 \text{ mm}^2$ . Its performance is evaluated using unit cell boundaries and Floquet ports in the CST electromagnetic solver. Upon satisfactory performance evaluation via simulations, these AMC unit cells are duplicated into the form of an array to form the AMC plane. Square patches are expected to result in a large bandwidth and fabrication simplicity [27]. This is validated by observing its phase response for the proposed AMC structure in Fig. 2(a). The larger bandwidth is due to its larger reflected surface area compared to the other two designs. This, however, will result in a larger AMC unit cell design relative to the cell spacing and resonant frequency.

To balance this trade-off, a smaller sized AMC with optimal bandwidth and reflection performance needs to be chosen. The proposed unit cell in this work combines the conventional square patch and the JSC slot for added compactness. It is dimensioned at  $7.75 \times 7.75 \text{ mm}^2$ , as depicted in Fig. 1(b). The JSC slot structure is then chosen to enable a larger net reflection surface area while simultaneously enabling miniaturization. The performance of the slotted JSC is also comparable to the other designs and is summarized in Table 1. The permittivity and permeability of the JSC slot unit cell with respect to the frequency shown in Fig. 2(b) was extracted using CST MWS simulator. From the imaginary part of permittivity and permeability, it is observed that both results are approximately zero within the operating band. Nevertheless, the JSC slot unit cell resulted in a high permeability and near to unity permittivity. Despite with an increased loss, a higher permeability will result in larger bandwidth.

To evaluate the effects of the PDMS and AMC plane with such layer configuration, three simple rectangular microstrip antennas were designed. The first antenna is a two-layered Taconic TLY-5 substrate, and this is set as the reference antenna (A1). The next two antennas are fabricated in a "hybrid" configuration, which consists of two layers, a layer of Taconic TLY-5 on as the top and PDMS as the bottom substrate. Antenna A2 is configured in this way, whereas antenna A3 is similar to A2 with an additional AMC layer (A3) between the PDMS and Taconic intersection. The substrates for all three substrates are identically dimensioned, whereas their patches are designed to operate at 9.41 GHz. This resulted in a different radiator sizes of  $11.8 \text{ mm} \times 11.8 \text{ mm}$  for A1,  $10.5 \text{ mm} \times 10.5 \text{ mm}$  for antenna A2 and  $4.1 \text{ mm} \times 3.5 \text{ mm}$  for the case of A3.

Fig. 3 compares the performance of the three antennas. It is observed that the bandwidth is increased to about 5.1% for the hybrid antenna (A2) compared to 4.5% bandwidth for the antenna on normal substrate (A1). Meanwhile, antenna A3 integrated with the PDMS and AMC plane indicated a larger bandwidth of nearly 8% (see Fig. 3(a)). Besides bandwidth, the combination of the AMC plane with the hybrid substrate resulted in a much higher 6.75 dB gain compared to the gain of 3.94 dB (for A2) and 4.12 dB (for A1), see Fig. 3(b). Note also that the antenna A1 has a higher maximum total efficiency of 91.3% at 9.41 GHz compared to A2 and A3 with 86.3% and 86.4%, respectively. This is due to the relatively higher material losses in the PDMS substrate. Nonethe-

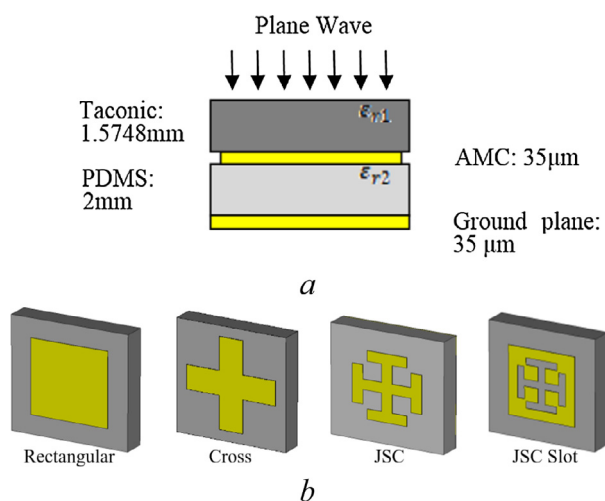


Fig. 1. AMC unit cell (a) setup, (b) AMC structures with proposed JSC Slot.

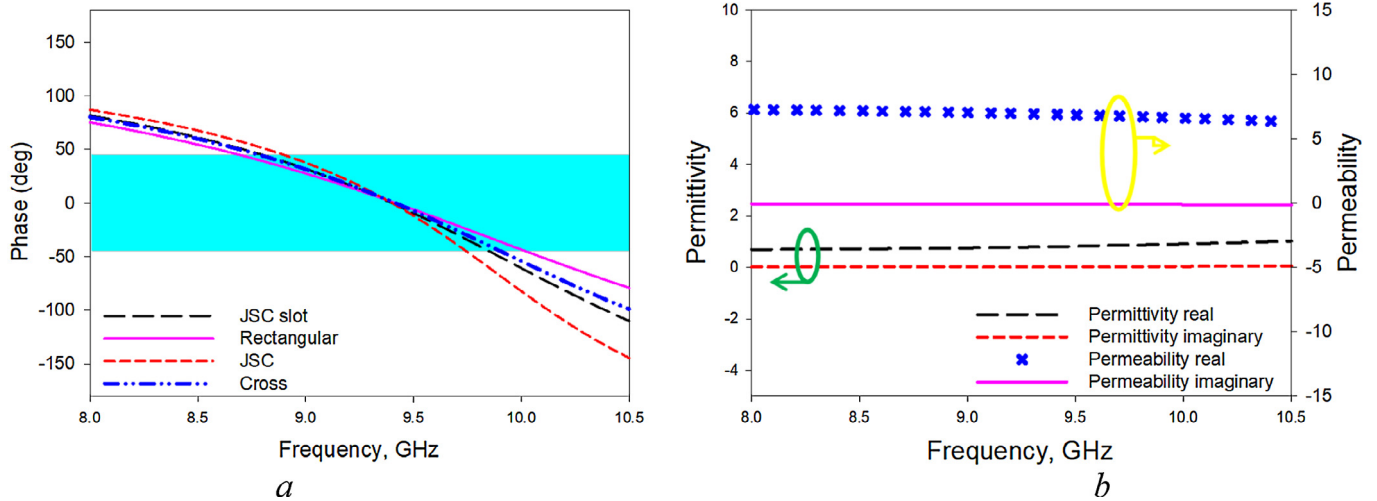


Fig. 2. The simulation results of (a) phase response of simulated AMC structures and (b) permittivity and permeability of simulated JSC slot.

Table 1  
Comparison of unit cell bandwidth and loss.

| Unit Cell    | $\pm 45^\circ$ Bandwidth (GHz) | Reflection loss (dB) | Size (mm <sup>2</sup> ) |
|--------------|--------------------------------|----------------------|-------------------------|
| Rectangular  | 1.32                           | 0.66                 | 8.85 × 8.85             |
| Cross        | 1.12                           | 0.74                 | 8.85 × 8.85             |
| JSC          | 0.84                           | 1.14                 | 8.85 × 8.85             |
| Proposed AMC | 1.05                           | 0.90                 | 7.75 × 7.75             |

less, the total efficiency of antenna A3 throughout the AMC bandwidth is at least 75%.

### 3. Integration of dipole antenna with AMC and MEMS

In this section, a planar dipole is chosen to further evaluate the effects of the AMC. The choice of this antenna is due to its omnidirectional behaviour and the absence of any large ground plane. The AMC is integrated on an E-shaped complementary planar dipole, which is designed based on a conventional folded dipole, see Fig. 4(a). The dipole arms are folded to ensure size miniaturization. To avoid the effect of line discontinuities, all 90° corners on the folded dipole are curved. At each ends of the complementary

E-Shaped dipole antenna arm, two parasitic elements with lengths of about  $0.3\lambda$  are placed with a spacing of  $15.6 \times 10^{-3}\lambda$  as depicted in Fig. 4(b). They act as the beam directors, enabling antenna steering towards a wider main lobe.

The main lobe is incorporated with the beam-reconfigurability feature by integrating two RF MEMS switches (model RMS101 from Radant) onto each arm of the folded dipole; see Fig. 4(b). The use of these two switches resulted in two beam configurations. Due to its matching limitations, the antenna will not operate during the simultaneous activation or deactivation of both switches. They are activated by injecting a 90 VDC signal into its gate pad. A layer of a AMC unit cell array is then placed between the two different substrate layers, see Fig. 4(c) and (d). The dimension of the proposed AMC is shown in Fig. 4(c). The overall structure is fed via a probe from the bottom-most layer, where a full ground plane is located, see Fig. 4(d).

The suitable AMC plane size and how it affects the performance of the proposed antenna is investigated as follows. Three AMC unit cell configurations,  $2 \times 3$ ,  $4 \times 3$  and  $6 \times 3$  are integrated onto a same antenna, see Fig. 5. They are denoted as AMC1 ( $2 \times 3$ ), AMC2 ( $4 \times 3$ ) and AMC3 ( $6 \times 3$ ). The size of this antenna is kept constant and compatible to the largest (AMC3) unit cell configura-

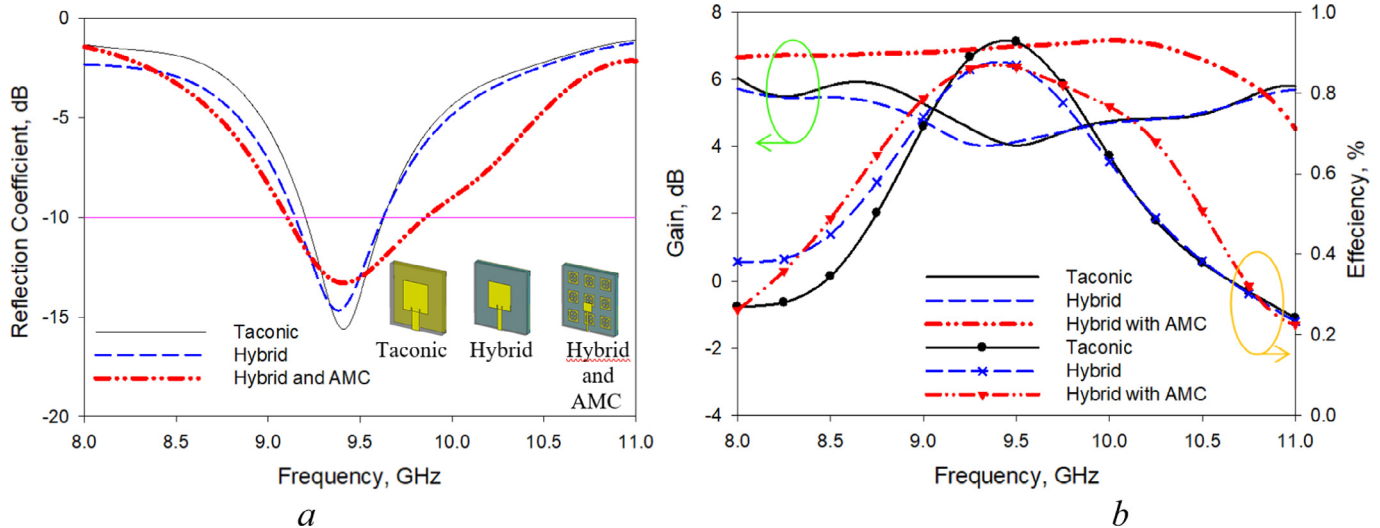


Fig. 3. Simulated results of the basic rectangular antenna: (a) reflection coefficient; and (b) gain and efficiency.

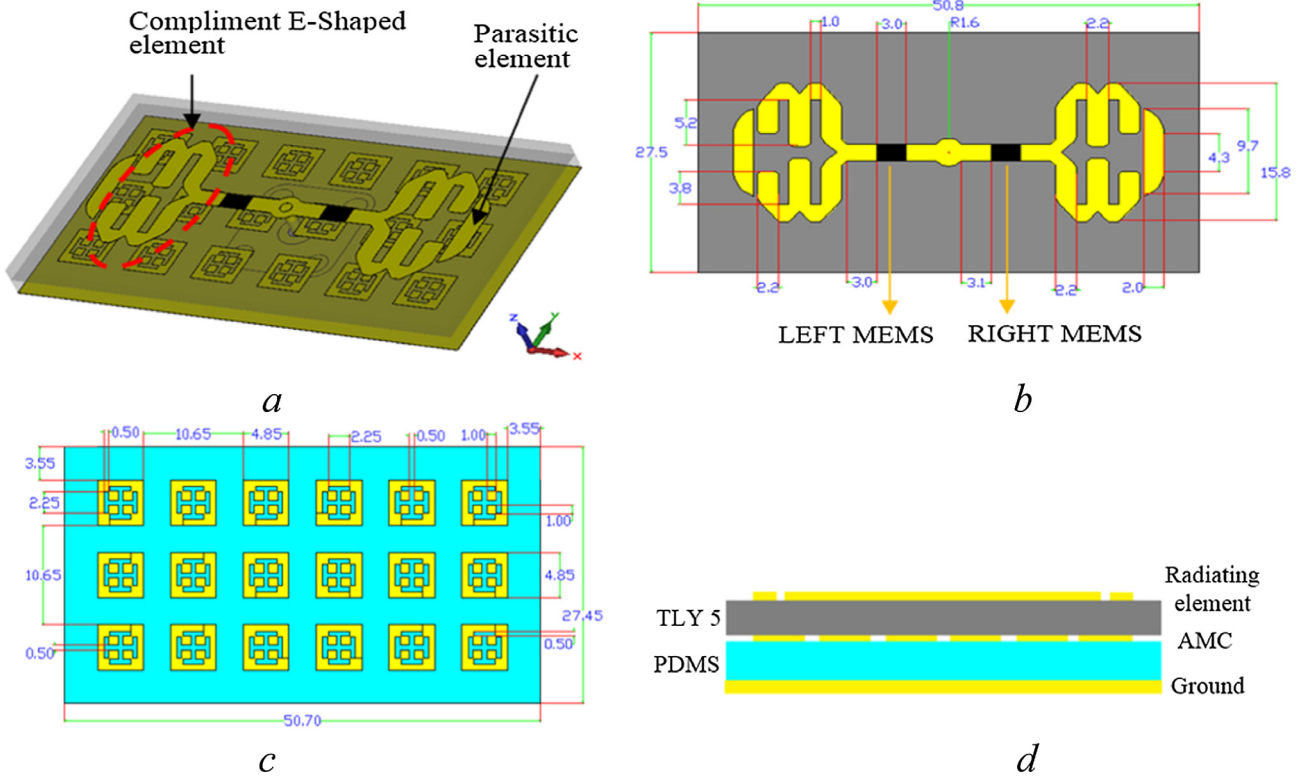


Fig. 4. Structure of the proposed antenna (unit in mm). (a) three dimensional (3D) view, (b) top view, (c) AMC plane, (d) side view.

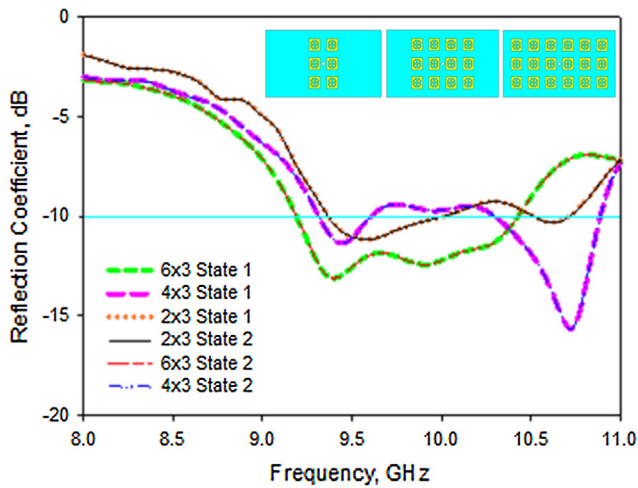


Fig.5. The three investigated simulated AMC configurations and their resulting reflection coefficients (same for State 1 and State 2 of the MEMS switches).

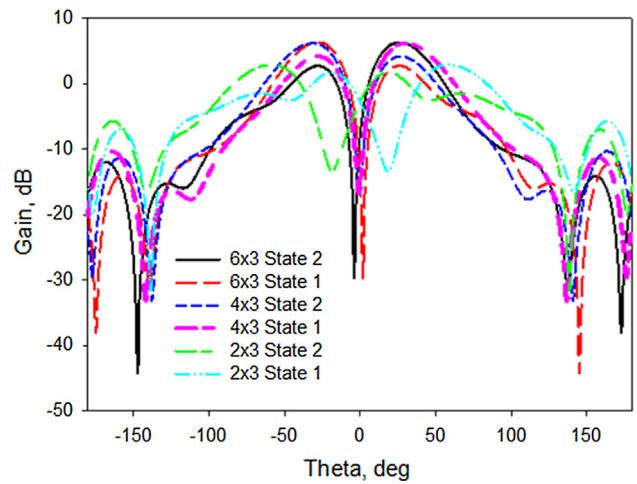


Fig.6. Simulated radiation patterns for two states of the proposed antenna loaded with AMC1, 2 and 3 (xz-plane).

tion. As shown in Fig. 5, the proposed antenna loaded with AMC1 operated at the frequency of 9.41 GHz with a bandwidth of 6.8%. Meanwhile, a dual band operation at 9.44 GHz and 10.72 GHz is observed for AMC2, with no more than 6% of impedance bandwidth in each band. Finally, the antenna with AMC3 resonated at 9.41 GHz with a bandwidth of 13.18%. For all three AMC configurations, the reflection coefficients produced by the two MEMS switching states are the same due to symmetric switch locations.

Fig. 6 illustrates the radiation pattern of the proposed antenna loaded with AMC1, 2 and 3. Fig. 6 shows that the AMC3-integrated antenna resulted in the same side lobes level as of AMC2. This indicates the effectiveness of plane's function as a perfect magnetic conductor (PMC) reflector at 9.41 GHz. However, the

half power beamwidth (HPBW) of the AMC3 is smaller compared to AMC2, which then leads to the higher gain. Besides that, the AMC2 configuration is also limited in terms of total efficiency. Meanwhile, AMC1 is the least suitable choice due to its poor performance in both aspects. The simulated total efficiency, main lobe direction, side lobe level and HPBW for all AMC and switch configurations are summarized in Table 2.

As mentioned above, the presence of the PDMS lowered resonances when the antenna is similarly sized, with enhancement in its bandwidth. The use of the PDMS layer also enabled the coverage of the full radio navigator and location bandwidth from 9.2 to 10 GHz. To determine the losses incurred from the MEMS switches, the proposed antenna has also been simulated and compared with

**Table 2**  
The effect of different AMC configurations on the antenna performance at 9.41 GHz.

| Quantity             | State      | AMC configuration |       |       |
|----------------------|------------|-------------------|-------|-------|
|                      |            | 6 × 3             | 4 × 3 | 2 × 3 |
| Gain (dB)            | Both state | 6.3               | 5.69  | 2.29  |
| Efficiency (%)       | Both state | 77.49             | 73.26 | 72.91 |
| HPBW (°)             | Both state | 34.4              | 36.7  | 44.8  |
| Main lobe (°)        | Both state | ±28               | ±29   | ±59   |
| Side lobe level (dB) | Both state | −3.9              | −3.9  | −1.2  |

an ideal switch. This switch is hypothetical in nature: a copper strip represents the ON state and an open circuit for the OFF state. As illustrated in Fig. 7(a), the radiation efficiency within its operating band for both states are similar. However, the total efficiency is slightly lower than the ideal case when using RF MEMS due to the expected losses of about 0.3 dB at 9.41 GHz. Nevertheless, the discrepancy is acceptable, with a maximum decrease of only 7%. The AMC plane maintained the proposed antenna gain at 9.41 GHz for both cases as shown in Fig. 7(b). The FBR for the antenna with MEMS is also lower than the ideal case due to its losses, as depicted in Fig. 7(b). However, the FBR using MEMS is more than 25 dB at 9.41 GHz.

**4. Results and discussion**

To provide a fair validation with the simulation results, the proposed antenna has been fabricated with the same dimension as optimized in simulation on the polymeric substrate. More details of the fabrication process is also explained in [33]. The measured

reflection coefficient,  $S_{11}$  for the fabricated antenna demonstrated in Fig. 8 is depicted in Fig. 9. Measured bandwidths are slightly smaller compared to simulations. Nevertheless, measured  $S_{11}$  between 9.1 GHz and 10 GHz is consistently below −10 dB. Moreover, the measured outcomes show a satisfactory agreement for both states. Table 3 compares the radiation patterns in the xz-plane at 9.41 GHz. Noted that the variance among the measured peak gain of the main lobe and side lobe is only about 5.31 dB. However, this is acceptable for a pattern-reconfigurable antenna [32]. The simulated-measured result discrepancies are due to several factors such as fabrication errors and variation in material tolerance. The substrate characteristics tolerance especially its thickness and permittivity must be considered with care as this will result in frequency shifting and gain degradation. Besides that, the additional cable of the prototype antenna purposely for activation and deactivation of the RF MEMS is placed near to the transmission line despite our best efforts to avoid this, see Fig. 8(c). This structure contributes to the difference between simulation and measurement outcomes. A comparison table to previous literature in terms of performance is presented in Table 4 to highlight the contribution of this proposed antenna.

**5. Conclusion**

In this paper, an AMC plane integrated with two modified folded dipole antenna on polymeric substrate (PDMS) is designed and investigated. A beam steering of 30° and −24° is demonstrated by integrating two RF MEMS on the proposed antenna. The presence of the AMC plane acts as a reflector and contributed to the effective suppression of back radiation. As a result, the antenna features a high FBR and maximum gain of about 18.66 dB and 5.11 dB,

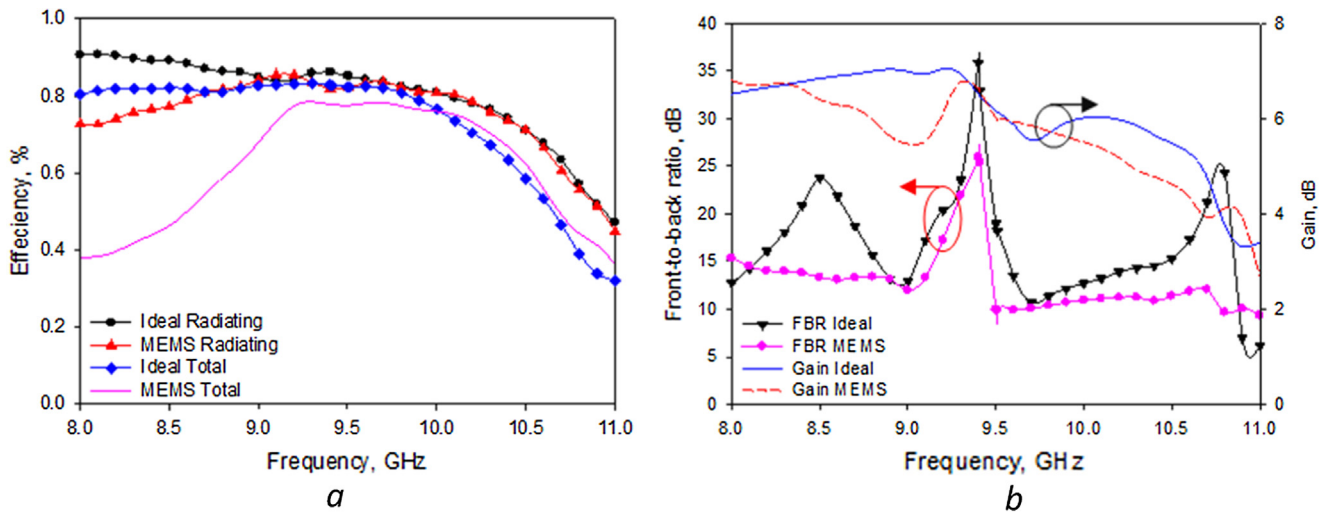


Fig. 7. Comparison between ideal and MEMS case in term of (a) radiation and total efficiency and (b) front-to-back ratio and gain.

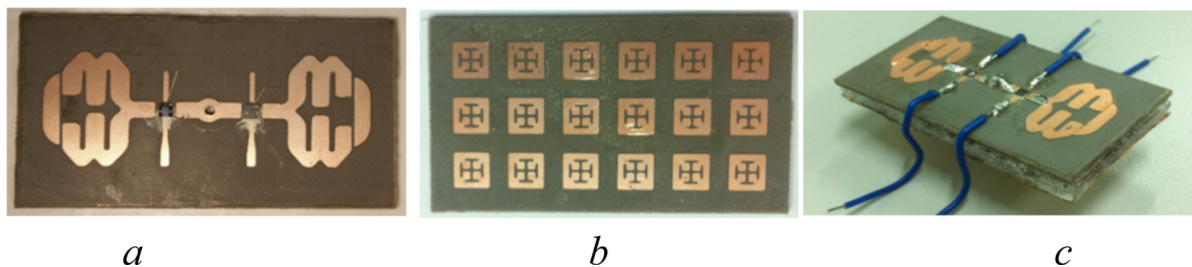


Fig. 8. The fabricated prototype (a) top view, (b) AMC plane, (c) perspective view.

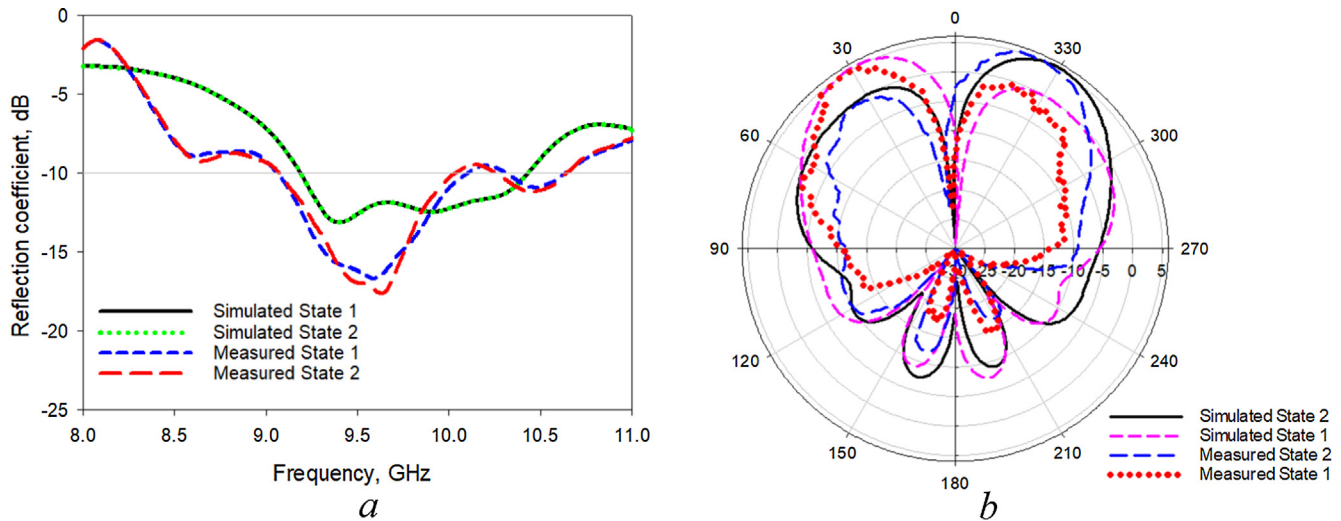


Fig. 9. (a) Simulated and measured antenna reflection coefficients and (b) measured radiation patterns in the xz-plane.

Table 3

Summary of the proposed antenna performance.

| Parameter                  | State   | Simulate | Measure |
|----------------------------|---------|----------|---------|
| Peak gain (dB)             | State 1 | 6.3      | 5.05    |
|                            | State 2 | 6.3      | 5.11    |
| Main lobe (°)              | State 1 | 28       | 30      |
|                            | State 2 | -28      | -24     |
| 10 dB operating band (GHz) | State 1 | 1.24     | 0.92    |
|                            | State 2 | 1.24     | 1.04    |

Table 4

Comparison with earlier related work of reconfigurable radiation pattern antennas integrated on metasurface.

| Antenna type                               | Frequency (GHz) | Electrical size of antenna (width × length × thickness)      | Beam steering technique | Maximum gain (dB) | Steering angle (°) | Bandwidth (GHz) |
|--|-----------------|--|-------------------------|-------------------|--------------------|-----------------|
| Normal circular patch with metasurface [2] | 5.5             | 70 × 70 × 3.05 mm <sup>3</sup><br>(1.28 × 1.28 × 0.06 λ)     | Mechanical              | 7.2               | ±32                | 0.2 (3.6%)      |
| Yagi-Uda like with HIS [21]                | 2.45            | 120 × 155 × 10.5 mm <sup>3</sup><br>(0.96 × 1.24 × 0.08 λ)   | Pin Diode               | 4.34              | ±50                | 0.06 (2.7%)     |
| Dipole with parasitic and AMC [19]         | 9.41            | 54.5 × 24.5 × 3.26 mm <sup>3</sup><br>(1.7 × 0.77 × 0.10 λ)  | MEMS                    | 8.08              | ±58                | 0.56 (5.95%)    |
| Proposed antenna                           | 9.41            | 50.8 × 27.5 × 3.68 mm <sup>3</sup><br>(1.59 × 0.86 × 0.12 λ) | MEMS                    | 5.11              | ±30                | 1.0 (10.6%)     |

respectively. Moreover, a large bandwidth of up to 1 GHz (10.6%) is realized by combining AMC and PDMS as substrate layers. The presented simulation and measurement results performed indicated satisfactory performance in terms of reflection coefficient and radiation patterns.

## Appendix A. Supplementary material

Supplementary data to this article can be found online at <https://doi.org/10.1016/j.aeu.2018.12.011>.

## References

- [1] Ding C, Guo YJ, Qin PY, Bird TS, Yang Y. A defected microstrip structure (DMS)-based phase shifter and its application to beamforming antenna. *IEEE Trans Antennas Propag* 2014;62:641–51. <https://doi.org/10.1109/TAP.2013.2290802>.
- [2] Zhu HL, Cheng SW, Yuk TI. Mechanically pattern reconfigurable antenna using metasurface. *IET Microwave Antennas Propag* 2015;9:1331–6. <https://doi.org/10.1049/iet-map.2014.0676>.
- [3] Ashchyshyn YY, Modelski JW. Rigorous analysis and investigations of the scan antennas on a ferroelectric substrate. *IEEE Trans Microwave Theory Technol* 2005;53:427–38. <https://doi.org/10.1109/TMTT.2004.840779>.
- [4] Edalati NA, Denidni TA. Frequency selective surface for beam-switching application. *IEEE Trans Antennas Propag* 2013;61:195–200. <https://doi.org/10.1109/TAP.2012.2219842>.
- [5] Rodrigo D, Cetiner BA, Jofre L. Frequency, radiation pattern and polarization reconfigurable antenna using a parasitic pixel layer. *IEEE Trans Antennas Propag* 2014;62:3422–7. <https://doi.org/10.1109/TAP.2014.2314464>.
- [6] Pringle LN, Harms PH, Blalock SP, Kiesel GN, Kuster EJ, Friederich PG, et al. A reconfigurable aperture antenna based on switched links between electrically small metallic patches. *IEEE Trans Antennas Propag* 2004;52:1434–45. <https://doi.org/10.1109/TAP.2004.825648>.
- [7] Kovitz JM, Rajagopalan H, Rahmat-Samii Y. Design and implementation of broadband MEMS RHCP/LHCP reconfigurable arrays using rotated E-shaped patch elements. *IEEE Trans Antennas Propag* 2015;63:2497–507. <https://doi.org/10.1109/TAP.2015.2417892>.
- [8] Gianvittorio JP, Rahmat-Samii Y. Reconfigurable patch antennas for steerable reflect array applications. *IEEE Trans Antennas Propag* 2006;54:1388–92. <https://doi.org/10.1109/TAP.2006.874311>.
- [9] Petit L, Dussopt L, Laheurte J-M. MEMS-switched parasitic -antenna array for radiation pattern diversity. *IEEE Trans Antennas Propag* 2006;54:2624–31. <https://doi.org/10.1109/TAP.2006.880751>.
- [10] Lago H, Jamlos MF, Aziz SZ, Rahman NA. A reconfigurable MEMS beam steering array (RMBSA) antenna for smart RADAR application. In: *IEEE Symposium*

- Wireless Technology Application (ISWTA), Kota Kinabalu, Sabah, 96–99, Nov 2014. p. 96–99. <https://doi.org/10.1109/ISWTA.2014.6981204>.
- [11] Khairnar VV, Kadam BV, Ramesha CK, Gudino LJ. A reconfigurable parasitic antenna with continuous beam scanning capability in H-plane. *AEU-Int J Electron Commun* May 2018;88:78–86. <https://doi.org/10.1016/j.aeue.2018.02.014>.
- [12] Narayan S, Sangeetha B, Sruthi TV, Shambulingappa V, Nair RU. Design of low observable antenna using active hybrid-element FSS structure for stealth applications. *AEU-Int J Electron Commun* Oct 2017;80:137–43. <https://doi.org/10.1016/j.aeue.2017.06.038>.
- [13] Qin P-Y, Guo YJ, Ding C. A beam switching quasi-yagi dipole antenna. *IEEE Trans Antennas Propag* 2013;61:4891–9. <https://doi.org/10.1109/TAP.2013.2274635>.
- [14] Donelli M, Azaro R, Fimognari L, Massa A. A planer electronically reconfigurable Wi-Fi band antenna based on a parasitic microstrip structure. *IEEE Antennas Wirel Propag Lett* 2007;6:623–6. <https://doi.org/10.1109/LAWP.2007.913274>.
- [15] Ren J, Yang X, Yin J, Yin Y. A novel antenna with reconfigurable patterns using H-shaped structures. *IEEE Antennas Wirel Propag Lett* 2015;14:915–8. <https://doi.org/10.1109/LAWP.2014.2387292>.
- [16] Bai Y-Y, Xiao S, Liu C, Shuai X, Wang B-Z. Design of pattern reconfigurable antennas based on a two-element dipole array model. *IEEE Trans Antennas Propag* 2013;61:4867–4871. <https://doi.org/10.1109/TAP.2013.2270175>.
- [17] Huff GH, Bernhardt JT. Integration of packaged RF MEMS switch with radiation pattern reconfigurable square spiral microstrip antennas. *IEEE Trans Antennas Propag* 2006;54:464–9. <https://doi.org/10.1109/TAP.2005.863409>.
- [18] Safari M, Shafai C, Shafai L. X-band tunable frequency selective surface using MEMS capacitive loads. *IEEE Trans Antennas Propag* 2015;63:1014–10121. <https://doi.org/10.1109/TAP.2014.2386304>.
- [19] Available: <<http://www.radantmems.com>>.
- [20] Lago H, Jamlos MF, Soh PJ, Vandenbosch GA. AMC-integrated reconfigurable beamforming folded dipole antenna with parasitic and RF MEMS. *Prog Electromagn Res C* 2016;69:159–67. <https://doi.org/10.2528/PIERC16082403>.
- [21] Li M, Xiao S-Q, Wang Z, Wang B-Z. Compact surface-wave assisted beam-steerable antenna based on HIS. *IEEE Trans Antennas Propag* 2015;62:3511–9. <https://doi.org/10.1109/TAP.2014.2321161>.
- [22] Vallecchi A, De Luis JR, Capolino F, De Flaviis F. Low profile fully planar folded dipole antenna on a high impedance surface. *IEEE Trans Antennas Propag* 2012;60:151–62. <https://doi.org/10.1109/TAP.2011.2167912>.
- [23] Akhondzadeh-Asl L, Kern DJ, Hall PS, Werner DH. Wide-bands dipoles on electromagnetic bandgap ground planes. *IEEE Trans Antennas Propag* 2007;55:2426–34. <https://doi.org/10.1109/TAP.2007.904071>.
- [24] Zhu S, Langley R. Dual-band wearable textile antenna on an EBG substrate. *IEEE Trans Antennas Propag* 2009;57:711–7. <https://doi.org/10.1109/TAP.2009.2014527>.
- [25] Mosallaei H, Sarabandi K. Antenna miniaturization and bandwidth enhancement using a reactive impedance substrate. *IEEE Trans Antennas Propag* 2004;52:2403–14. <https://doi.org/10.1109/CIINFES.2014.7036623>.
- [26] Yan S, Soh PJ, Vandenbosch GA. Low-profile dual-band textile antenna with artificial magnetic conductor plane. *IEEE Trans Antennas Propag* 2014;62:6487–90. <https://doi.org/10.1109/TAP.2014.2359194>.
- [27] Cook BS, Shamim A. Utilizing wideband AMC structure for high-gain inkjet-printed antennas on lossy paper substrate. *IEEE Antennas Wirel Propag Lett* 2013;12:76–9. <https://doi.org/10.1109/LAWP.2013.2240251>.
- [28] Joubert J, Vardaxoglou JC, Whittow WG, Odendaal JW. CPW-fed cavity-backed slot radiator loaded with an AMC reflector. *IEEE Trans Antennas Propag* 2012;60:735–42. <https://doi.org/10.1109/TAP.2011.2173152>.
- [29] Abbasi NA, Langley RJ. Multiband-integrated antenna/artificial magnetic conductor. *IET Microwave Antennas Propag* 2011;5:711–7. <https://doi.org/10.1049/iet-map.2010.0200>.
- [30] Alqadami ASM, Jamlos MF, Lago H, Babarinde OJ. Bandwidth enhancement of microstrip antenna array using magneto-dielectric polymer substrate (PDMS-Fe3O4). In: *IEEE Symposium Wireless Technology Application (ISWTA)*, Kota Kinabalu, Sabah, 152–155, Nov 2014. <https://doi.org/10.1109/ISWTA.2014.6981177>.
- [31] Lago H, Jamlos MF, Hamid MR. Beam steering printed dipole antenna on incorporate of polymeric and HIS. In: *RF and Microwave Conference (RFM)*, 2015 IEEE International. IEEE; 2015. p. 183–5. <https://doi.org/10.1109/RFM.2015.7587740>.
- [32] Qin P-Y, Guo YJ, Weily AR, Liang C-H. A pattern reconfigurable U-slot antenna and its application in MIMO system. *IEEE Trans Antennas Propag* 2012;60:516–28. <https://doi.org/10.1109/TAP.2011.2173439>.
- [33] Alqadami ASM, Jamlos MF, Soh PJ, Vandenbosch GA. Assessment of PDMS technology in a MIMO antenna array. *IEEE Antennas Wirel Propag Lett* 2016;15:1939–42. <https://doi.org/10.1109/LAWP.2015.2513960>.